Temperature Regimes and Chemistry for Stabilizing Precipitation Hardening Phases in Al–Sc Alloys: Combined CALPHAD–Deep Machine Learning

Rajesh Jha
Department of Mechanical and Materials Engineering; MAIDROC Laboratory,
Florida International University,
10555 West Flagler Street,
Miami, FL 33174
e-mail: rjha001@fiu.edu

George S. Dulikravich[1]
Fellow ASME
Department of Mechanical and Materials Engineering,
MAIDROC Laboratory,
Florida International University,
10555 West Flagler Street,
Miami, FL 33174
e-mail: dulikrav@fiu.edu

In this work, CALPHAD-based calculations provided with data for various stable and metastable phases in 2XXX, 6XXX, and 7XXX classes of aluminum-based alloys. These data were scaled and then used to develop Deep Learning Artificial Neural Network (DLANN) models for all these phases as a function of composition and temperature. Code was written in the PYTHON programming language using TensorFlow/Keras libraries. DLANN models were used for determining the amount of various phases for new compositions and temperatures. The resulting data were further analyzed through the concept of Self-organizing Maps (SOM) and a few candidates were chosen for studying the precipitation kinetics of Al_3Sc phase under the framework of CALPHAD approach. This work reports on heat-treatment simulation for one case of 6XXX alloy where the nucleation site was on dislocation, while a detailed study for other alloys is reported in a previously published work. Grain-growth simulations presented in this work are valid for single crystals only.
[DOI: 10.1115/1.4054368]

Keywords: advanced materials and processing simulation, CALculation of PHase Diagram (CALPHAD) approach, face centered cubic (FCC), Kampmann–Wagner Numerical (KWN) approach, artificial intelligence/machine learning, data-driven design, design of engineered materials system, innovative material synthesis and manufacturing methods, metallic materials, microstructure property relationships

1 Introduction

Aluminum is one of the most abundant elements in the Earth's crust and has the potential of replacing steel and titanium alloys in the automotive and aerospace sector due to its superior strength-to-weight ratio [1]. One of the challenges is to develop aluminum alloys than possess superior mechanical properties and are corrosion resistant at elevated temperatures of about 400 °C. Aluminum alloy series 2XXX is Al-Cu based, 6XXX is Al-Mg-Si based, while 7XXX is Al-Mg-Zn based [1]. Initial classifications of 2XXX, 6XXX, and 7XXX were based on a particular alloying element as mentioned below [1]. However, these alloys can contain several alloying elements. The precipitation sequence of critical phases in these alloys is as follows:

- 2XXX: Supersaturated solid solution transforms to GP-zones which further transforms into θ'' followed by θ' which finally transforms into a stable θ (Al_2Cu) phase. This class of alloys achieves superior strength when θ'' and θ' are predominant [1].
- 6XXX: Supersaturated solid solution transforms to GP-zones which further transforms into β'' followed by β' which finally transforms to stable β (Mg_2Si) phase. Here, the predominant phase is β'', which is observed after aging [1].
- 7XXX: Supersaturated solid solution transforms to GP-zones which further transforms into η' which finally transforms to stable η (Mg_2Zn) phase. This class of alloys achieves superior strength when η' and η are predominant while maximum hardness is achieved when η' is predominant [1].

In aluminum-based alloys, all the metastable as well as the stable phases can be present in the microstructure [2,3]. However, in thermodynamic calculations, one may not observe any trace of metastable phases in the presence of a stable phase [3].

Scandium (Sc) improves mechanical strength and corrosion resistance of aluminum alloys, and the Al_3Sc phase is thermodynamically stable [1,4–6]. However, scandium is expensive and it can form a stable Al_3Sc phase up to a saturation limit [1]. Thus, scandium can be added up to a certain amount, while the above-mentioned metastable phases still are beneficial for achieving superior mechanical properties in these alloys. Aluminum alloys with scandium addition may need two-step aging as Al_3Sc precipitates during aging at temperatures between 300 °C and 450 °C, while other metastable phases precipitate around 200 °C [1]. Research shows [5] that Al_3Sc dispersoids can be helpful in nucleation and stabilization of θ' phase precipitates during aging. At the same time, an increase in copper content has a dual effect on coarsening of Al_3Sc precipitates, as the increase in copper content can lead to both increase and decrease of coarsening of Al_3Sc precipitates [7]. Thus, it is important to study the effect of composition and temperature on the stability of stable and metastable phases in aluminum alloys with scandium addition.

[1]Corresponding author.
Manuscript received November 19, 2021; final manuscript received April 11, 2022; published online May 9, 2022. Assoc. Editor: Mark M. Derriso.

Aluminum (Al) alloys have been studied under the framework of the CALPHAD approach [8–11] using Thermo-Calc software [3,12–14]. The available literature on aluminum alloys studied through the CALPHAD approach deals with compositions of known alloys or slight deviations from known compositions [8–11]. Additionally, the number of elements in these alloys is relatively small and varies between 3 and 8 maximum [8–11].

Thus, the current research problem was framed so that it can address the current limitations. In the work presented here, alloys have been considered to have 12 alloying elements for 2XXX, 10 elements for 6XXX, and 11 elements for 7XXX, thus expanding the number of alloying elements of the current state of the art.

Through the CALPHAD approach, one can only estimate the stable phases. A phase associated with minimum Gibbs free energy will be the most stable for a given composition and temperature regime. Any other phase with a Gibbs free energy higher than that phase will be unstable or metastable, and its amount cannot be estimated through equilibrium calculations for that given composition and temperature regime. In multicomponent systems like the present case of aluminum alloy, there exist several metastable phases which are important for improving multiple mechanical properties of that alloy. In order to estimate those metastable phases, one has to suppress stable phases while performing equilibrium calculations. They must repeat these calculations multiple times in order to estimate these metastable phases. Through deep learning artificial neural network (DLANN), a user can use the data generated through the CALPHAD approach and develop the DLANN model for each of these phases. Thereafter, they can estimate all of these phases for thousands of new compositions in a fraction of a second, while these calculations may take hours through the CALPHAD approach.

In the current work, data were generated through the CALPHAD approach [3,12–14] for various stable and metastable phases for 2XXX, 6XXX, and 7XXX families of alloys to explore the optimum scandium content that can be beneficial for precipitation of the Al_3Sc phase along with other stable and metastable phases. These data were then used to develop predictive models for each of these stable and metastable phases as a function of composition and temperature [15]. A computer code was developed in the PYTHON programming language using TensorFlow [16] and Keras [17] libraries to develop Deep Learning Artificial Neural Network (DLANN) models for each of the stable and metastable phases in 2XXX, 6XXX, and 7XXX classes of aluminum alloys. These predictive DLANN models were then used to predict stable and metastable phases for new compositions and temperatures. Thereafter, these data were used and analyzed through Self-organizing Maps (SOM) [18–20] to determine various patterns within the dataset as well as for choosing a few candidate alloy compositions to perform solidification and heat-treatment simulations under the framework of the CALPHAD approach. In the current work, one case of isothermal heat-treatment simulation for 6XXX alloy is reported where the nucleation site is at the dislocations. Detailed studies of solidification and heat-treatment simulations have been reported in another publication [15]. Our research group has expertise in designing alloys' compositions for optimal properties by the application of several concepts of artificial intelligence on data generated through experiments and data generated under the framework of the CALPHAD approach [18–24]. This publication is intended to provide researchers with a predictive tool for screening alloy compositions for phase stability prior to performing experiments.

2 Materials and Methods

In this study, 2XXX, 6XXX, and 7XXX classes of aluminum alloys were chosen. These classes of alloys are heat treatable. For each class of these alloys, variable bounds for concentrations of alloying elements were defined based on data available in the literature [1,4]. These variable bounds for the chemical composition of alloy series 2XXX, 6XXX, and 7XXX are reported in Table 1. It can be observed that in 2XXX a total of 12 alloying elements were considered. In the 7XXX series, the addition of Zr along with Sc was considered, while dropping V, while for the 6XXX series alloys both Zr and V were excluded. Equilibrium calculations were performed to stabilize the metastable phases for these alloys.

Table 1 Minimum and maximum concentrations for each of the 12 alloying elements (wt%) for three series of Al–Sc-based alloys (also reported in Ref. [15], reprinted with permission from Elsevier)

	2XXX Series		6XXX Series		7XXX Series	
Element	Min.	Max.	Min.	Max.	Min.	Max.
Si	0.20	1.20	0.20	1.80	0.12	0.50
Fe	0.30	0.50	0.10	0.70	0.15	0.50
Cu	3.80	6.80	0.10	0.40	0.10	2.40
Mn	0.20	1.20	0.05	1.10	0.05	0.70
Mg	0.02	1.80	0.35	1.40	0.80	3.70
Cr	0.00	0.10	0.00	0.35	0.00	0.30
Zn	0.10	0.25	0.05	0.25	3.80	8.30
Ti	0.02	0.15	0.00	0.20	0.01	0.20
V	0.00	0.15	0.00	0.00	0.00	0.00
Zr	0.00	0.25	0.00	0.00	0.00	0.20
Sc	0.00	10.00	0.00	10.00	0.00	10.00
Al	Balance to 100.00		Balance to 100.00		Balance to 100.00	

2.1 Identification of Stable and Metastable Phases. Commercial software, Thermo-Calc 2018B [12], was used for studying stability of phases using the thermodynamic database TCAL5 [3] and mobility database MOBAL4 [14]. Assadiki et al. [25] provided a brief description of stabilizing metastable phases in aluminum alloys, which can be useful for studying 2XXX and 6XXX alloys. As mentioned before, in 2XXX supersaturated solid solution transforms to GP-zones which further transform into θ'' followed by θ' which finally transforms into a stable θ (Al_2Cu) phase. Thermodynamic database TCAL5 [3] and Andersen et al.'s [26] study on various precipitates in aluminum alloys show that θ'' closely resembles GPII zones in 2XXX, while θ-Al_2Cu is the stable phase. In 6XXX, β'' closely resembles GPII zones in 2XXX, while β-Mg_2Si is the stable phase [3,26]. For 7XXX, η-$MgZn_2$ is the stable phase with the C14 structure, while η' is the metastable phase [27]. In the thermodynamic database TCAL5 [3], V_PHASE is considered as $MgZn_2$, while there exists another phase with C14_LAVES_PHASE in the TCAL5 database. The structure of the GP-zones or η' phase has been debated [26]. In the thermodynamic database TCAL5 [3], Al_3Sc exists as the AL3X phase. CALPHAD approach utilizes Gibbs Energy minimization as a criterion to determine the formation and stability of any particular phase [12,25]. In Thermo-Calc [12], it is possible not to get another metastable phase in 2XXX, 6XXX, and 7XXX, although it can coexist with the stable phases experimentally [3].

2.2 Generation of Phase Stability Data. The prime target phase, Al_3Sc, is the stable phase. But, in aluminum alloys, superior properties are achieved by the combination of stable and metastable phases. For stabilizing metastable phases, one needs to suppress the stable phases during equilibrium calculations. This way the next phase becomes stable and its amount (volume fraction and mole fraction) can be estimated. For example, for the 2XXX series, 1200 sets of compositions and temperature were generated and amounts (volume fraction) were estimated of the θ (AL2CU_C16) phase. For these 1200 cases, no metastable phases were observed. Therefore, the θ (AL2CU_C16) phase was removed from calculation and generated 1200 sets of compositions and temperature for which again the amount of θ' phase was calculated through Thermo-Calc. This way, a significant amount of data was generated for

stable and metastable phases for 2XXX alloys. The dataset includes 1200 combinations of composition and temperature for each of the stable and metastable phases. Similarly, a large amount of data was generated for the 6XXX and 7XXX series of alloys that is suitable for the application of various concepts of artificial intelligence.

2.3 Data Preprocessing. Data obtained from Thermo-Calc were not directly used. All these data were scaled. It will be mentioned in the main body of the article.

2.4 Deep Learning Artificial Neural Network (DLANN) Template. *This is a multicomponent system with multiple design variables.* Specifically, there are 10–12 alloying elements and temperature as variables in a design process using data generated through Thermo-Calc and developed predictive models for each of the stable and metastable phases as a function of the concentration of alloying elements and temperature. Computer code was written in the PYTHON programming language using TensorFlow [16] and Keras [17] libraries for developing DLANN models for each of these stable and metastable phases as a function of alloying elements and temperature for 2XXX, 6XXX, and 7XXX alloys.

Prior to model development, data were scaled for all the variables and objectives such that all values were between 0 and 1. Variables include composition and temperature of candidate alloys, and objectives are the amount of stable and metastable phases. There were several cases for which the equilibrium amount of phase was 0 (zero). This is a complex dataset where too many points are missing. A Deep Learning Artificial Neural Network (DLANN) was then developed which had four hidden layers. The architecture of the DLANN is something that a user decides. For example, the first hidden layer consisted of 50 neurons, and the remaining three layers consisted of 100 neurons each. For each of the alloying phases studied here, a DLANN was developed where the initial layer was set as having 50, 60, 70, 80, 90, or 100 neurons, while each of the other three hidden layers consisted of 100, 120, 140, 160, 180, or 200 neurons, respectively.

This dataset was divided randomly into a training set for training the DLANN model and a testing set for its validation. The testing set consisted of 33% of all the available data mainly to avoid overfitting. Rectified Linear Unit (ReLU) was chosen as the activation function, while "AdaM" was chosen as an optimizer [16,17]. AdaM stands for Adaptive Moment Estimation. The stopping criterion for training was the number of epochs, and it was fixed at 100 for all of these cases. Mean Squared Error (MSE) and Mean Absolute Error (MAE) over the validation set was one of the performance metrics considered for choosing a model for various stable and metastable phases. Tensorboard [28] was used for visualization and determining/choosing the model that can be used for predictive tools. Apart from MAE/MSE error metrics and visualization *via* Tensorboard, the most important criterion for choosing a model was the physical metallurgy of aluminum alloys. In this work, there are lots of missing data points for metastable phases. This requires giving priority to the physical metallurgy of aluminum alloys. Thus, concepts of statistics and artificial intelligence are used as a guiding tool, while avoiding overdependence on these tools.

As mentioned, Al_3Sc is a stable phase, while there are several stable and metastable phases. Through the CALPHAD approach, both stable and metastable phases cannot be estimated simultaneously for a given composition and temperature. Separate calculations need to be performed for estimating both stable and metastable phases. Hence, DLANN models were used to estimate the amount of stable and metastable phases for compositions and temperature in equilibrium in case any of this information was missing. These estimates were performed for 2XXX, 6XXX, and 7XXX series alloys. Hence, a more complete dataset was created containing all the stable and metastable phases in equilibrium for any given chemical composition and temperature.

2.5 Self-Organizing Maps. Data obtained from DLANN models for various phases were then analyzed through the concept of SOM [18–20] for understanding patterns, correlations among variables, correlations between variables and the number of critical phases, and correlations among the critical phases. SOM plots are known for preserving the topology of the dataset. SOM maps are used to determine complex correlations in large and small datasets and are known for preserving the topology of the dataset, though the prediction capability of SOM is not accurate as each of the hexagonal units on the SOM plots are averaged [18–20]. In this approach, accurate predictive DLANN models were developed through the Deep Learning approach. Hence, SOM analysis was used for analyzing correlations and studying patterns within the dataset.

Through SOM analysis, a set of candidate alloys was selected based on the optimum amount of stable and metastable phases for 2XXX, 6XXX, and 7XXX alloys. SOM analysis of 6XXX alloys has been reported in the main paper, while SOM analysis of 2XXX and 7XXX series alloys is reported in Appendix A.

2.6 Solidification and Heat-Treatment Simulations. The chemical composition of the candidate alloys was used for studying the precipitation kinetics of the Al_3Sc phase, where the nucleation sites were in the bulk. Most of this work has been reported in other publications [15]. In the current work, a case for 6XXX series Al-based alloys is presented where isothermal heat-treatment simulations were performed at 300 °C and the nucleation sites were at the dislocations. Interfacial energy between the precipitate (AL3X) and the matrix (FCC_L12) was optimized for this simulation. It was fixed at 0.07 J/m^2. Thermo-Calc module TC-PRISMA uses Kampmann–Wagner Numerical (KWN) [8] approach for simulating precipitation kinetics. Governing equations for KWN approach have been included in Appendix B and the companion paper [15].

2.7 Computational Infrastructure

2.7.1 CALPHAD-Based Work. Thermo-Calc was installed on a desktop computer in a computer lab. The operating system was Windows 10, Core i7 processor (CPU) with 16-GB random access memory (RAM). Phase transformation calculation time varied between 20 min and 30 min, depending on the number of alloying elements considered for an alloy system. As mentioned, 12 elements were considered for 2XXX alloys, 10 elements for 6XXX, and 11 elements for 7XXX series of Al-based alloys. For heat- treatment simulation presented in this work, it took about 3 to 4 h. In this work, heat-treatment simulations for 6XXX alloys were performed with 10 elements where the nucleation sites were on dislocation. During this simulation with the nucleation site on dislocation, the system crashed comparably more often than when performing simulations with nucleation sites in the bulk [15].

2.7.2 Artificial Intelligence-Based Work. Artificial Intelligence (AI)-based work was performed on a laptop. The operating system was Windows 10, Core i7 processor (CPU) with 32 GB RAM. DLANN model development took about 20–30 min depending on the number of alloying elements. Once the model was developed, the prediction was done in a few seconds. DLANN models were also used on an Android phone with 6 GB RAM and octa-core processor (CPU). Prediction time was a few seconds on the Android phone. SOM model development took about 20–30 min for each case.

3 Results

3.1 DLANN Model. Based on the literature [3,26–29] and the developed DLANN model, performance metrics for models for various phases in 2XXX, 6XXX and 7XXX series alloys has been listed in Table 2.

Table 2 Performance metrics for DLANN models for various phases in 2XXX, 6XXX, and 7XXX series of Al-based alloys

			Error metrics (validation set)	
Alloy	Phase	DLANN Architecture	Mean square error (MSE)	Mean absolute error (MAE)
2XXX	THETA_PRIME (θ')	90-180-180-180	4.47e-4	0.01535
	THETA_DPRIME (θ'')	60-120-120-120	9.87e-4	0.01972
	AL2CU_C16 (θ)	80-160-160-160	0.01086	0.04221
	S_PHASE	50-100-100-100	4.24E-4	0.01077
	AL3X (Al_3Sc)	80-160-160-160	6.69e-4	0.0207
6XXX	MG2SI_C1(β)	70-140-140-140	6.63e-4	0.01911
	BETA_PRIME (β')	80-160-160-160	8.32e-4	0.0175
	BETA_DPRIME (β'')	80-160-160-160	1.79e-3	0.01075
	AL3X (Al_3Sc)	80-160-160-160	6.09e-4	0.01898
7XXX	C14_LAVES (η')	50-100-100-100	6.63e-4	0.01892
	T_PHASE	100-200-200-200	1.56e-3	0.01877
	V_PHASE (η-$MgZn_2$)	80-160-160-160	8.31e-3	0.04712
	S_PHASE	50-100-100-100	1.76e-3	0.01604
	AL3X (Al_3Sc)	60-120-120-120	2.13e-5	2.9961e-3

The architecture of the DLANN model chosen in this work has been listed in Table 2. The Mean Absolute Error (MAE) in Table 2 appears to be large at first glance. As mentioned in Sec. 2.3, data for all the design variables and objectives were scaled between 0 and 1. DLANN models were developed for all the stable and metastable phases as a function of composition and temperature. From phase stability data, it could be observed that the maximum amount (mole fraction) of any of these phases was numerically low (about 0.1). Mole fraction value for any of these phases varied between 0 and 0.1.

Regarding the error metrics in Table 2, apart from AL2CU_C16 (θ), mean square errors (MSE) for all the phases are quite low, on the order of 1e-3 to 1e-5. AL2CU_C16 (θ) and V_PHASE (η-$MgZn_2$) have a mean absolute error (MAE) of about 0.4. Most of the MAE values for other phases are around 0.01, while MAE for AL3X for 7XXX series is extremely small, of the order of 1e-3. MAE of around 0.01 still seems large. However, when these models will be used as a predictive tool, these results will be rescaled back to provide a practical estimate of the amount of all these phases. For example, the initial range (0–0.1) was scaled to a new range (0–1) for model development. After these models are used for prediction, these data will be rescaled, or the range (0–1) will be scaled back to the range (0–0.1). Thus, even if considering MAE at 0.01, after rescaling it will become 0.001. In a complex problem with 10–12 alloying elements and a large database with several missing values, an error of 0.001 can be acceptable, though there is still room for improvement. Again, it should be recalled that in this work artificial neural network (ANN) model with four hidden layers was developed through Deep Learning approach. ANN models are prone to overfitting. Thus, one must be careful while choosing a model and using it as a predictive tool. As mentioned before, priority was given to physical metallurgy of aluminum alloys in selecting DLANN models, while using concepts of statistics and artificial intelligence for guidance. AL2CU_C16 (θ) data contain lots of missing values, and there are 13 variables: temperature and concentrations of 12 alloying elements. For MAE at 0.04, it will be rescaled to 0.004. MAE is about 4% when compared with the maximum value for AL2CU_C16 (θ), which is about 0.1. Thus, although MAE and MSE appear large for a few cases, they are still between 1% and 5% of the maximum value, which is still quite small for a complex problem like this.

One can observe that the chosen model has a different structure, where 50–100–100–100 represents the number of neurons in the four hidden layers of the DLANN. Based on our experience, DLANN models with acceptable performance metrics MSE and MAE, calculated over the validation/testing set, were chosen for further study. A reader needs to take into account that there were several cases where the amount of phase is zero, and the alloy system contains 9–12 alloying elements. From the data sheet, 67% of data were assigned to the training set and 33% of data were assigned to the testing set, mainly to avoid overfitting. Hence, there is a possibility to improve the performance metrics of the models by changing these parameters.

Table 3 SOM Error metrics for 2XXX, 6XXX, and 7XXX series of Al–Sc-based alloys

	Quantization error	Topological error
2XXX	0.126	0.030
6XXX	0.109	0.034
7XXX	0.131	0.017

3.2 Self-organizing Maps Analysis. Table 3 summarizes the error metrics of SOM analysis for 2XXX, 6XXX, and 7XXX alloys. It can be observed in Table 3, that topological error is low, while quantization error is comparatively higher. In this work, predictive models were developed through TensorFlow/Keras libraries in PYTHON [16,17] with better prediction accuracy (Table 2). Thus, SOM was used for understanding patterns in the dataset, while for prediction, the Deep Learning Artificial Neural Network (DLANN) models were used. As mentioned before, a commercial software Thermo-Calc was used so that phase stability calculations were performed within the framework of the CALPHAD approach.

The CALPHAD approach utilizes Gibbs Energy minimization as a criterion to determine the formation and stability of any particular phase [12,25]. In aluminum alloys (2XXX, 6XXX, and 7XXX), targeted properties are achieved by an optimum combination of stable and metastable phases. Thermodynamically, these metastable phases will be absent in the presence of stable phases, but kinetically these metastable phases have been observed in the microstructure of aluminum alloys [2,3]. In order to stabilize a metastable phase, one needs to remove the stable phases while performing calculations for the stability of metastable phases. In this work, a complex multicomponent system for 2XXX, 6XXX, and 7XXX series alloys was chosen. It can be possible that a certain metastable phase can be absent for a certain composition and temperature combination

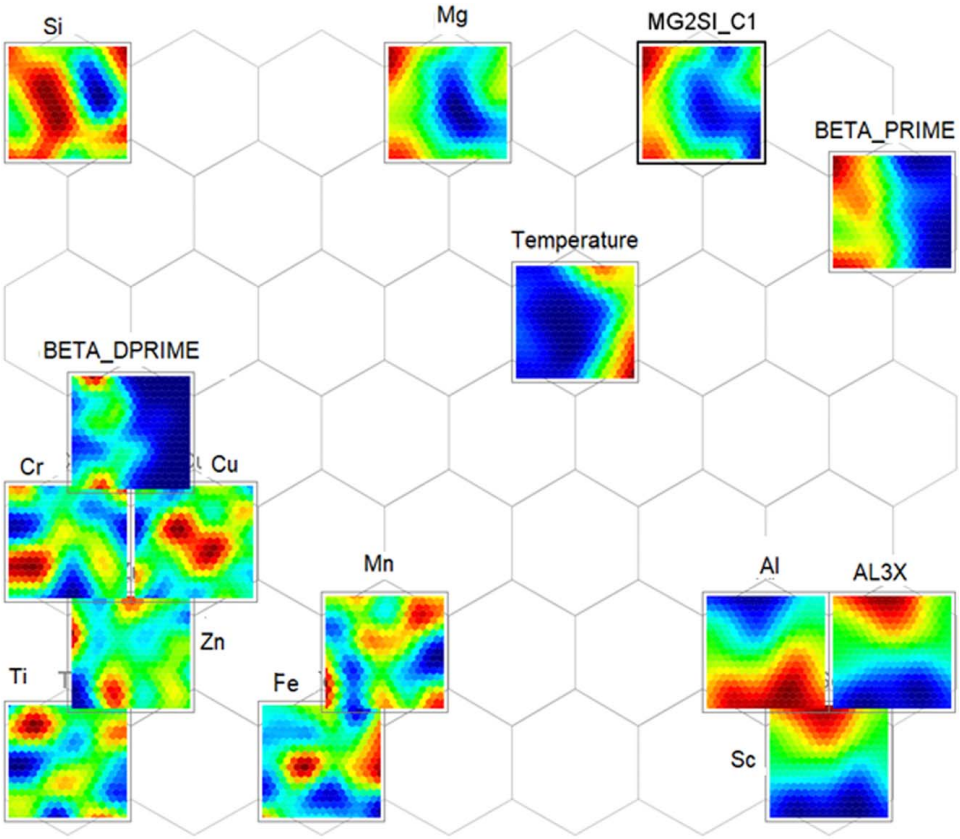

Fig. 1 SOM plot of components for alloying elements, and critical phases in 6XXX series of Al-based alloys along with Sc and temperature

even after the stable phases are removed from the calculation as several other equilibriums exist in a multicomponent system. Determining these compositions and temperature regimes can be helpful in screening alloys prior to performing experiments. Thus, SOM plots can be used to determine the composition regime prior to performing precipitation kinetics simulations for the Al_3Sc phase or experiments.

3.3. 6XXX Alloys. Figure 1 shows the component plot for 6XXX alloys. In Fig. 1, one can observe that elements Al, Sc, and the phase AL3X are clustered together or are correlated. This relation can be established as an increase in Al and Sc will lead to an increase in AL3X (Al_3Sc) phase. In Fig. 1, MG2SI_C1 (β) and BETA_PRIME (β') phases are clustered together. From the physical metallurgy of aluminum alloys, one can establish this relation as BETA_PRIME (β') is a metastable phase, which finally transforms into a stable MG2SI_C1 (β) phase [1].

Figure 2 shows the distribution of Sc, temperature, and a few critical phases for 6XXX series. SOM maps consist of hexagonal cells. Values visible on SOM maps are the average value over a cell. Hexagonal cells are not visible in Fig. 2 since a significantly large number of candidate alloys are included in this study; thus, the SOM map looks pixelated.

In Fig. 2, BETA_PRIME (β') and BETA_DPRIME (β"') exist in the lower temperature regime (~180 °C) and is nonexistent at elevated temperature (540 °C). Additionally, MG2SI_C1 (β) phase exists in a larger amount in a lower temperature regime (~180 °C). From the physical metallurgy of aluminum alloys, BETA_PRIME (β') and BETA_DPRIME (β'') are the metastable phases that finally transform into the thermodynamically stable MG2SI_C1 (β) phase [1]. Additionally, MG2SI_C1 (β), BETA_PRIME (β'), and BETA_DPRIME (β'') phases are stable in the temperature regime around 200 °C and are unstable at elevated temperatures [1]. SOM maps were able to recognize this pattern and correctly positioned the candidate alloys on the vertices of hexagonal units in a way that the predictions can be verified through concepts of physical metallurgy. Even though the SOM algorithm does not operate on principles of physical metallurgy, still it was able to mimic these vital correlations. This proves the efficacy of the application of SOM maps in materials design as in this problem the database contains several missing points, which is quite common in materials/alloy design problems. In Fig. 2, one can additionally observe that elements aluminum, scandium, and AL3X phase are correlated. An increase in aluminum and scandium results in an increase in the AL3X phase, which can be understood as the Al3X phase, in this case, is Al_3Sc.

One of the goals of this work is to determine the scope of working with small concentrations of Sc since Sc is expensive. From Fig. 2, it can be observed that it is possible to work with a lower amount of Sc (<wt. 2%) at lower temperatures since BETA_PRIME, BETA_DPRIME, and MG2SI_C1 phases are stable. Heat treatment of aluminum alloys in the case of Sc addition is performed in two stages. The annealing temperature for precipitating BETA_PRIME, BETA_DPRIME, and MG2SI_C1 phases is performed at around 100–200 °C, while the annealing temperature for precipitating AL3X is usually above 300 °C. Thus, SOM maps proved to be helpful in determining candidates for performing solidification and heat-treatment simulations. Based on the preceding computational effort, the most promising Al–Sc-based alloy from each of the three Al-based series (2XXX, 6XXX, and 7XXX) was selected for heat-treatment simulation as reported in Table 4. Candidates reported in Table 4 are also reported in Ref. [15], where simulations were performed for solidification and heat treatment for studying the precipitation kinetics of the Al_3Sc phase for these candidate alloys [15]. These compositions were obtained from artificial

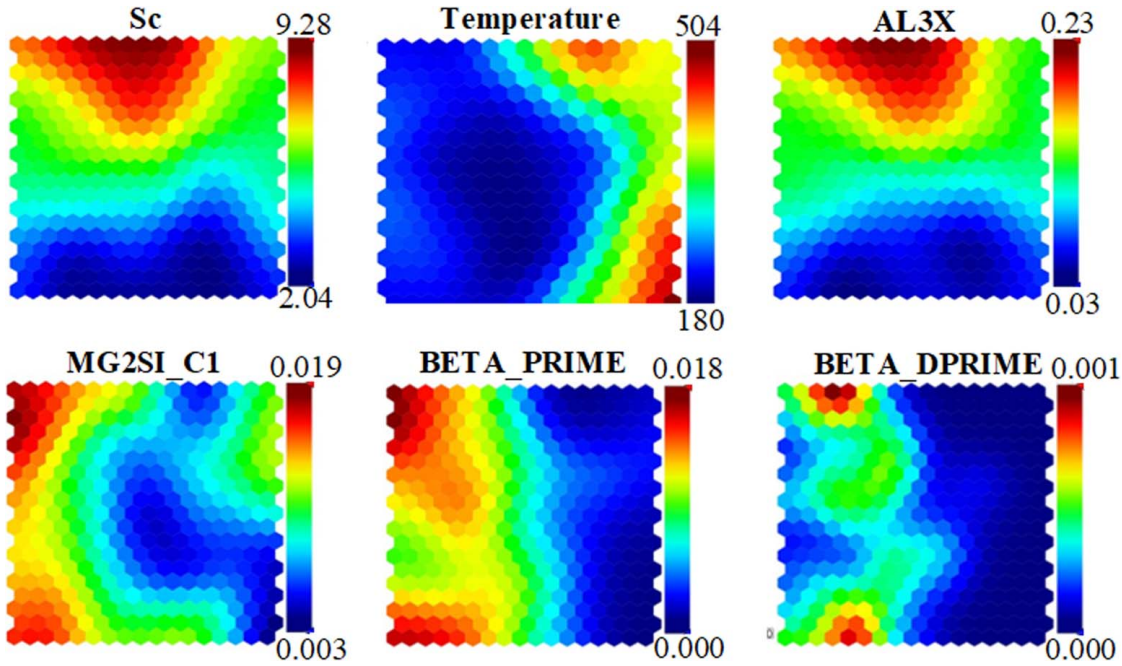

Fig. 2 Amount of critical phases (mole) in 6XXX series of Al-based alloys along with Sc (wt%) and temperature (°C)

intelligence-based algorithms. Practically, it is not possible to achieve similar compositions as shown in Table 4.

3.3.1 Heat-Treatment Simulations. In Ref. [15], simulations were performed where nucleation sites for precipitation of Al_3Sc phases were in the bulk. In the current work, precipitation kinetics simulation of the Al_3Sc phase was at the nucleation site which is at the dislocations. A candidate alloy corresponding to the 6XXX series from Table 4 was used, and isothermal annealing was performed at the dislocations at 300 °C. A system of 10 alloying elements, and no reported information on interfacial energy for such a complex system. In this work, the reference temperature was chosen as 300 °C. In Ref. [15], temperatures were chosen between 300 °C and 450 °C, where all the nucleation sites were in the bulk. Figure 3(*a*) shows the variation of the mean radius of the grain over the annealing time, which was set at 1000 h. Figure 3(*b*) shows the variation of volume fraction over annealing time. From Figs. 3(*a*) and 3(*b*), it can be observed that the mean radius and volume fraction of Al_3Sc crystals increase initially and saturate at about 67 h. After 67 h, there is minimal change in the growth of Al_3Sc crystals. Interfacial energy was optimized by trials and in this case, it was set at 0.07 J/m^2. For the optimal grain size of the Al_3Sc phase at dislocations, available literature [1] was consulted. Depending on the application, Al_3Sc grain size can vary from 2 to 100 nm. Strengthening in aluminum alloys is achieved by precipitation hardening and also mechanical working. In this work, dislocation density was fixed at 6.0×10^{12} m^{-3}. The mechanical treatment introduces many dislocations in the system. Thus, studying the precipitation kinetics of Al_3Sc crystals with dislocations as a nucleation site will be helpful for researchers working on aluminum alloys. In Ref. [15], the mean radius of the crystals increases continuously when the nucleation sites were in the bulk. In this work, nucleation sites are at the dislocations. A detailed analysis at other temperatures will be helpful to quantify the effect of time on overall grain size.

Table 4 Compositions (wt%) of three series of Al-based alloys chosen for solidification and heat-treatment simulation in a previously published work [15] (reprinted with permission from Elsevier)

Alloying element	2XXX Series	6XXX Series	7XXX Series
Si	0.38828	1.5497	0.28606
Fe	0.3919	0.57313	0.21862
Cu	4.95088	0.27893	1.51113
Mn	0.32005	0.63697	0.36188
Mg	0.53321	1.07076	1.05662
Cr	0.04353	0.1437	0.12353
Zn	0.19235	0.11882	3.73898
Ti	0.04297	0.13088	0.15506
V	0.09389	0.0	0.0
Zr	0.21774	0.0	0.17829
Sc	0.92541	2.60077	0.75953
Al	91.89979	92.89525	91.61031

4 Discussion

In this work, the research problem was formulated in a way which will be helpful in expanding the domain of the current state of the art or available literature on aluminum alloys studied under the framework of the CALPHAD approach.

The novelty of this work can be summarized in a few points as follows:

- Literature on aluminum alloys using the CALPHAD approach usually focuses on compositions which are around the known compositions of standard alloys [25]. In this work, a framework was developed to predict and test novel compositions through a thorough investigation based on the CALPHAD and Artificial Intelligence. Novel compositions can be analyzed through DLANN models and the equilibrium amount of various stable and metastable phases can be estimated in 2XXX, 6XXX, and 7XXX classes of aluminum alloys through this approach.
- Literature on aluminum alloys using the CALPHAD approach usually focuses on alloys with 6–8 alloying elements [4–11,25–29]. In this work, 12 alloying elements were considered for the 2XXX alloy system, 10 alloying elements for 6XXX, and 11 alloying elements for 7XXX series Al-based alloys, which will be helpful for researchers to utilize the presented approach in their own work, providing room for the addition of new elements in their existing alloys.

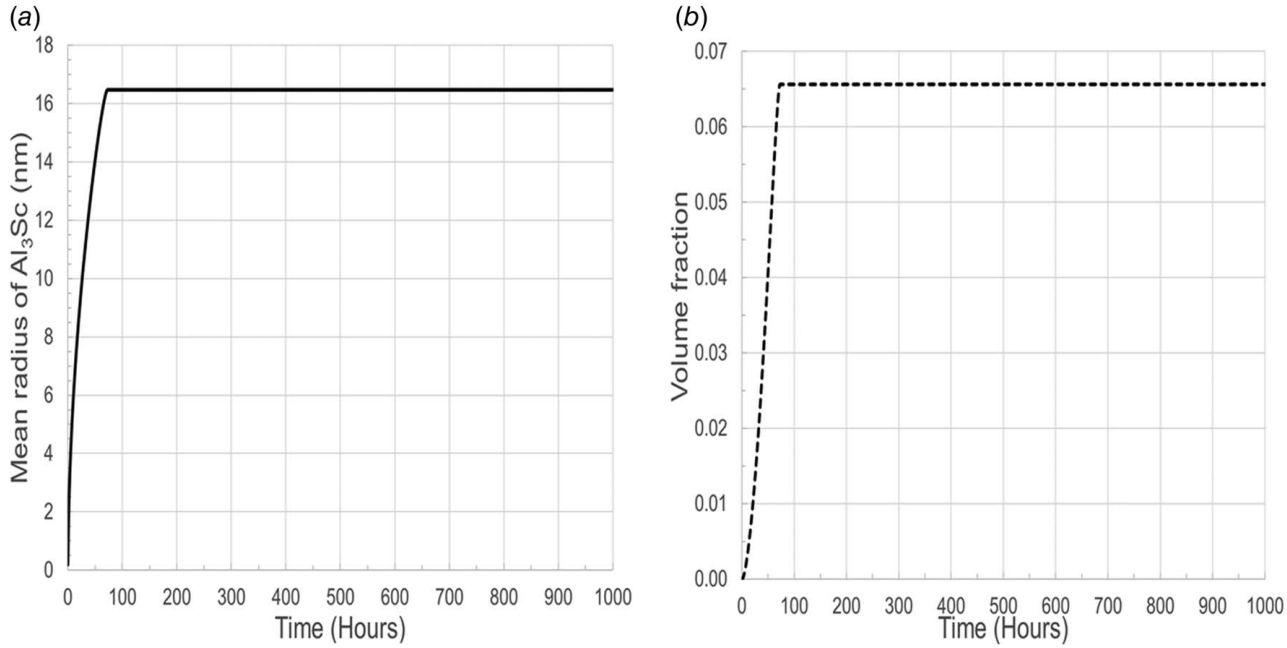

Fig. 3 Precipitation kinetics of Al_3Sc phase at dislocation for isothermal annealing at 300 °C for 6XXX series in Table 4: (*a*) mean grain radius (nm) and (*b*) volume fraction

- Scandium is added to aluminum alloys along with zirconium [30,31] and has a profound effect on mechanical properties in aluminum alloys. Both elements contribute to improvement in strength, hardness, and stress corrosion resistance. [30,31]. In a previously published work [15], alloys containing Zr were considered for Scheil solidification simulation and precipitation kinetic simulation of the Al_3Sc phase [15]. The current work is mainly focused on determining novel compositions for 2XXX, 6XXX, and 7XXX alloys while determining the scope of Sc addition. Heat-treatment simulation performed in this work is for the 6XXX alloy in Table 4, which does not contain any zirconium. This work cannot be compared with Refs. [30,31] as Zr containing alloy was not considered for heat-treatment simulation. A previously published work [15] can be compared to some extent.
- Solidification and heat-treatment simulations were performed and have been reported in a previously published work [15]. In the current work, precipitation kinetics simulation results with the nucleation site at the dislocation have been included. Isothermal annealing was performed at 300 °C. For the 6XXX alloy in Table 4, interfacial energy was optimized, and the value is 0.07 J/m2. From Fig. 3, it can be observed that the grain growth occurs in the beginning till about 67 h. After 67 h, grain size becomes stable as even up to 1000-h annealing time there is minimal change in grain size.

Heat-treatment simulations require optimized values of interfacial energy between precipitate and the matrix phase in order to mimic experimental findings, which is a must from an application point of view. Thus, our planned future work will focus on optimizing [20] interfacial energy at various nucleation sites for multicomponent aluminum alloys with scandium addition.

5 Conclusions

This study presents a novel computational approach that can be utilized for screening candidate alloys prior to performing experiments by estimating the equilibrium amount of various stable and metastable phases in aluminum alloys containing scandium. In this work, Deep Learning Artificial Neural Network (DLANN) was developed by utilizing a database generated for various stable and metastable phases for aluminum alloys under the framework of the CALPHAD approach. CALPHAD (Thermo-Calc) databases are created from actual experiments and atomistic simulations, while DLANN models were developed under the framework of TensorFlow/ Keras libraries that are known for determining nonlinear and complex correlations. The presented approach provides predictive DLANN models that can be used for new chemical compositions and temperatures to determine stable and metastable phases in the alloys at the same instant, as experimentally these phases coexist, but thermodynamically stable and metastable phases cannot coexist. Thereafter, data predicted through DLANN models were utilized to study 2XXX, 6XXX and 7XXX series Al–Sc-based systems and the stable and metastable phases in each of these systems by utilizing Self-Organizing Maps (SOMs). SOMs are known for determining complex correlations between design variables and objectives and also correlations among the objectives. Models developed through TensorFlow/Keras libraries have low error and SOM analysis of these alloys also shows low topological error. Based on this work, a few of the most promising chemical compositions requiring low concentrations of Sc were developed for performing heat-treatment simulations.

Solidification and heat-treatment simulations were performed on candidate alloys listed in Table 4 and had been reported [15]. In the current work, heat-treatment simulations for 6XXX alloy at 300 °C were performed where the nucleation sites were at dislocations. From the results, it can be observed that the average grain size stabilizes at about 67 h, and there is minimal change in grain size afterward even when isothermal simulations were performed for 1000 h. In this case, interfacial energy for the Al_3Sc phase was optimized. The presented work forms the basis for future work on optimizing interfacial energy for various nucleation sites. Grain-growth simulations presented in this work are valid for single crystals only.

Acknowledgment

The authors would like to express their sincere gratitude to Professor Cristian Ciobanu from the Colorado School of Mines for providing access to some of the commercial software used in this paper. Thanks, are also due to Professor Carlo Poloni from ESTECO Company for approving the free use of ESTECO's software modeFrontier in this research.

Funding Data

- This work was supported by the College of Engineering and Computing at Florida International University and by NASA HQ University Leadership Initiative (ULI) program under federal award number NNX17AJ96A titled "Adaptive Aerostructures for Revolutionary Supersonic Transportation" managed by Texas A&M University.

Conflict of Interest

There are no conflicts of interest. This article does not include research in which human participants were involved. Informed consent is not applicable. This article does not include any research in which animal participants were involved.

Data Availability Statement

Raw data set and developed models are for internal use and cannot be shared with this article.

Appendix A

2XXX Alloys. Figure 4 shows the component plot for 2XXX alloys, where all the variables (composition and temperature) and the objectives (critical phases) are positioned in a way that if any two or more of them are together, it means that they are correlated. This information is beneficial for an experimentalist in understanding the correlations between various design variables and objectives simultaneously. In Fig. 1 and Fig. 4, one can observe that elements Al, Sc, and the phase AL3X are clustered together or are correlated. This relation can be established as an increase in Al and Sc will lead to an increase in AL3X (Al_3Sc) phase. In Fig. 4, THETA_PRIME (θ') and THETA_DPRIME (θ'') phases are clustered together. From the physical metallurgy of aluminum alloys, one can establish this relation as metastable phase THETA_DPRIME (θ'') transforms into another metastable phase THETA_PRIME (θ'), which finally transforms into stable AL2CU_C16 (θ) phase. It should be mentioned that the SOM algorithm has no information on Gibbs energy minimization, the theory on which these databases predict a certain phase. Still, the SOM algorithm is able to capture information shown in the literature [1]. Alloying elements such as Si, Zr, Zn, Mn, Fe, Cr, Ti, and V are present in small amounts and are clustered together on the map. The alloy system under consideration is a complex multicomponent system, where the metastable phases were stabilized by suppressing the stable phases. Still, vital information on the interaction between components, components and various phases, and interaction between different phases were obtained through SOM analysis. Thus, it is possible to utilize SOM to determine the composition regime where a researcher can study precipitation kinetics of the Al_3Sc phase.

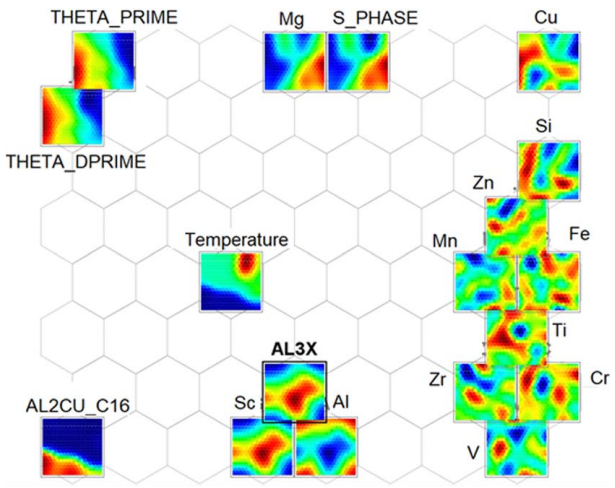

Fig. 4 SOM plot of components for alloying elements, and critical phases in 2XXX series of Al-based alloys along with Sc and temperature

Figure 5 shows the distribution of Sc, temperature, and a few critical phases for the 2XXX series. From Fig. 5, one can observe that Sc directly affects the amount of AL3X phase at all temperatures. Phase AL2CU_C16 is a thermodynamically stable phase, while THETA_PRIME and THETA_DPRIME metastable phases. In Fig. 5, THETA_PRIME, THETA_DPRIME, and AL2CU_C16 phases are stable at lower temperatures, which is also reported in the literature [1]. In Fig. 5, it can be additionally observed that THETA_PRIME and THETA_DPRIME are stable to a certain extent at moderate temperatures (above 200 °C), while AL2CU_C16 is absent for this temperature regime. Here, 200 °C is the average temperature of candidate alloys included in those SOM cells. Hexagonal cells are not visible since there are too many candidate alloys included in this study; thus, the SOM map looks pixelated. Any region on the SOM map that is marked above 200 °C consists of alloys for which the average temperature is above 200 °C. Heat treatment for precipitating Al_3Sc (AL3X) is performed at 300 °C or above, while for precipitating THETA_PRIME and THETA_DPRIME, heat treatment is performed below 200 °C. Thus, the occurrence of a few candidate alloys with a significant amount of THETA_PRIME and THETA_DPRIME will be helpful in designing new heat-treatment protocols for these classes of alloys. SOM algorithm proved to be useful in understanding various features/correlations in the dataset that can be validated by concepts of physical metallurgy of aluminum alloys. This demonstrates the efficacy of pattern recognition through SOM maps.

7XXX Alloys. Figure 6 shows the component plot for 7XXX alloys. It can be observed from Fig. 6 that AL3X, Sc, and Al are adjacent to each other. Thus, SOM plots were able to detect correlations between the concentrations of Al, Sc, and stable phase AL3X. One can also observe that minor elements like Si, Zr, Mn, Fe, Cr, and Ti are clustered together on the map. There does not seem to be any other strong correlations between design variables and desired phases, as C14_LAVES and V_PHASE are close, but not close enough to draw any definitive conclusion. Figure 7 shows the distribution of Sc, temperature, and a few critical phases for 7XXX series. From Fig. 7 it can be observed that Sc directly affects the amount of AL3X phase at all temperatures. C14_LAVES, V_PHASE and S_PHASE is stable at a lower temperature, marked around 170 °C on the SOM map. Above 170 °C, stability decreases for these phases. Here 170 °C is the average temperature for the candidate alloys included in the hexagonal units or cells. Thus, it can be possible that for a number of candidate alloys there can be traces of these phases and for a few candidates these phases can be in a larger or acceptable amount from a metallurgical point of view. This information will be helpful in designing new chemical compositions and manufacturing protocols for these alloys.

Figure 7 shows the distribution of Sc, temperature, and a few critical phases for the 7XXX series. From Fig. 4 it can be observed that Sc directly affects the amount of AL3X phase at all temperatures. C14_LAVES, V_PHASE, and S_PHASE are stable at a lower temperature, marked around 170 °C on the SOM map. Above 170 °C, stability decreases for these phases. Here, 170 °C is the average temperature for the candidate alloys included in the hexagonal units or cells. Thus, it can be possible that for a number of candidate alloys, there can be traces of these phases and for a few candidates these phases can be in a larger or acceptable amount from a metallurgical point of view. This information will be helpful in designing new chemical compositions and manufacturing protocols for these alloys.

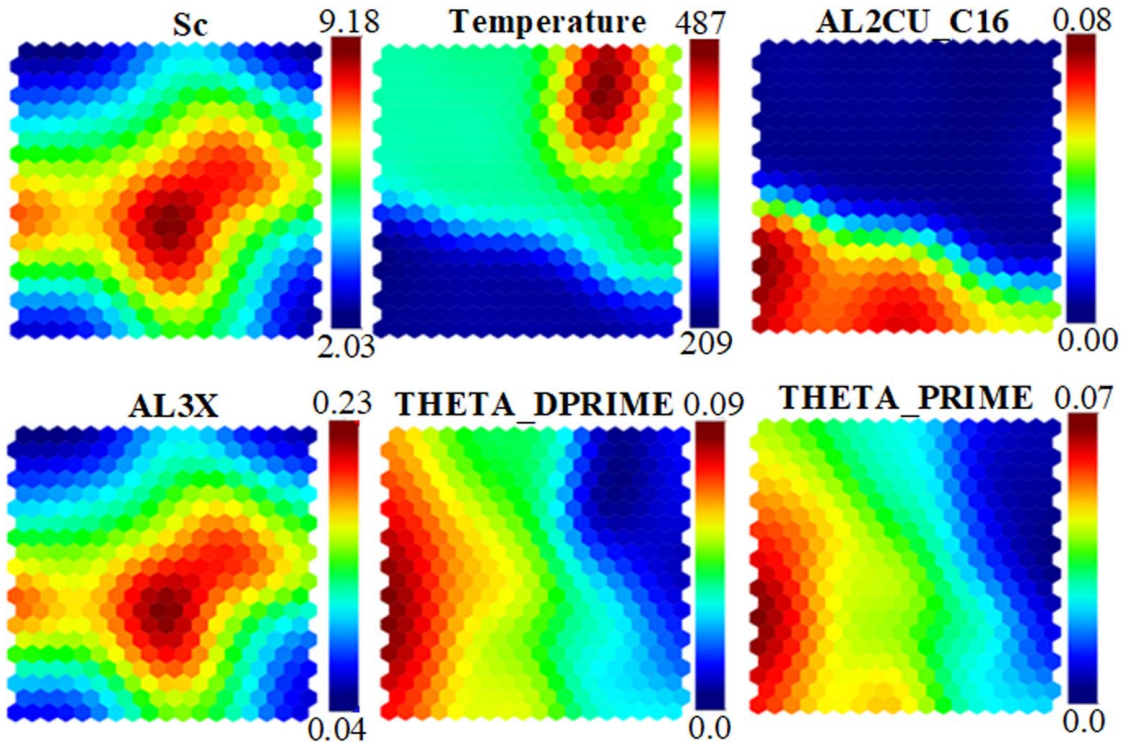

Fig. 5 Amount of critical phases in 2XXX series of Al-based alloys along with Sc and temperature

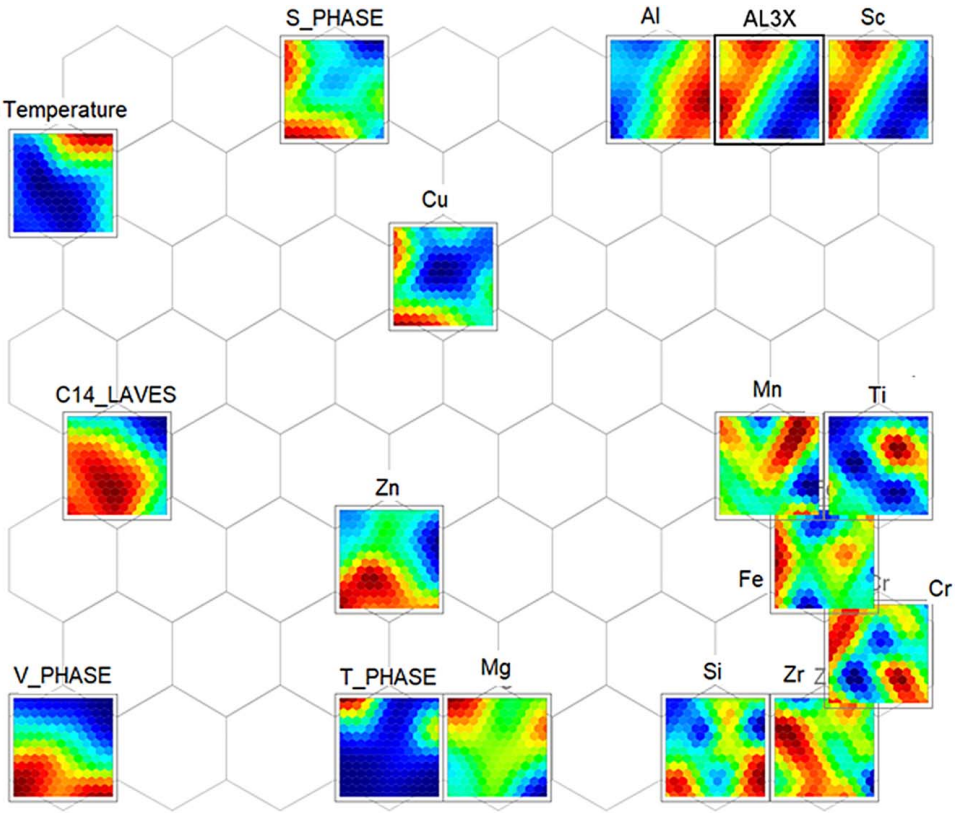

Fig. 6 SOM plot of components for alloying elements, and critical phases in 7XXX series of Al-based alloys along with Sc and temperature

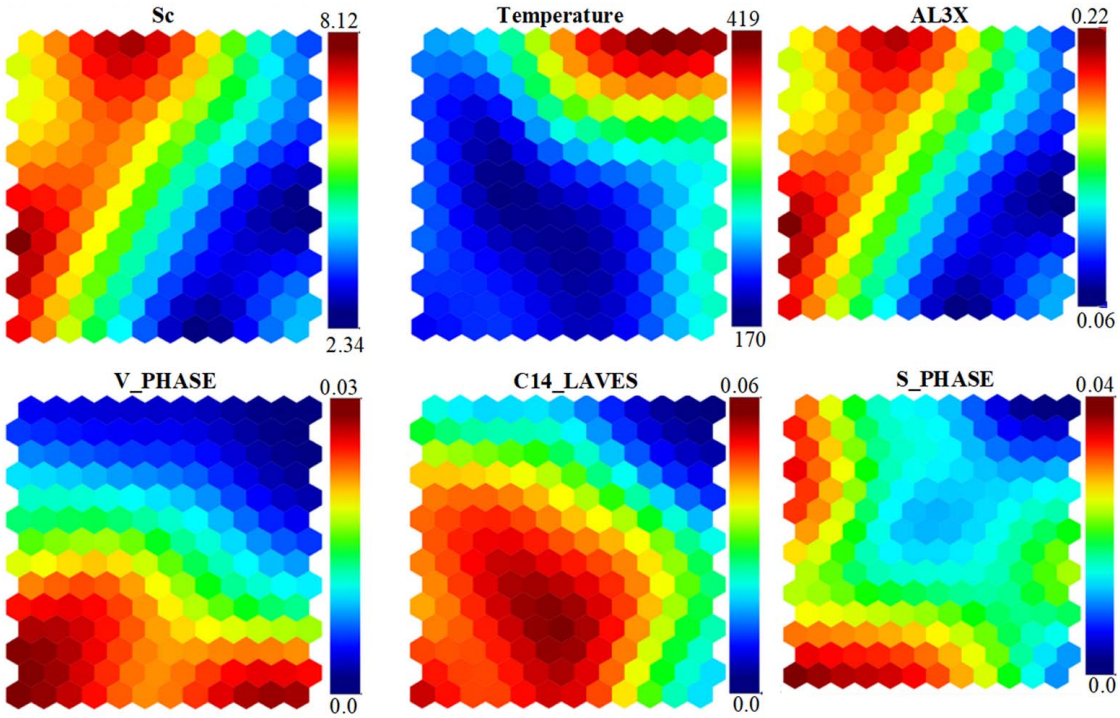

Fig. 7 Amount of critical phases in 7XXX series of Al-based alloys along with Sc and temperature

One of the goals for this work was to explore the possibility of Sc addition in small amounts (<2 wt%). Through this work, it became possible to find the compositions and temperature regimes for which Al_3Sc (AL3X) and other stable and metastable phases are stable in significant amounts. Based on the preceding computational effort, the most promising Al–Sc-based alloy from each of the three Al-based series was selected for heat-treatment simulation as reported in Table 4 in the main article and also in a previously published work [15].

Appendix B

Kampmann–Wagner Numerical Approach. TC-PRISMA module [13] in Thermo-Calc [12] utilizes the KWN approach for simulating precipitation kinetics of a precipitate which involves nucleation, growth, and coarsening [32–36]. This section explained the governing equations and lists the parameters used while simulating precipitation kinetics.

In this work, the matrix is the FCC_L12 phase. The precipitate is AL3X, which is Thermo-Calc notation for Al_3Sc. The molar volume of the precipitate was taken from the Thermo-Calc database. The grain aspect ratio was fixed at 1.0, while the mobility enhancement factor was fixed at 5.

An initial number of nucleation sites (N_0) were calculated from dislocation density, which was fixed at $6.0\times10^{12}/m^3$. Interfacial energy was set at 0.07 J/m^2.

Time-dependent nucleation rate (J_t) can be derived from classical nucleation theory [37] and is expressed as in Eq. (B1)

$$J_t = J_s \exp\left(\frac{-\tau}{t}\right) \tag{B1}$$

In Eq. (B1), τ is incubation time which can be further simplified as shown in Eq. (B2), t is the time and J_s is the steady-state nucleation rate as shown in Eq. (B3) [37–40]

$$\tau = \frac{1}{\theta Z^2 \beta^*} \tag{B2}$$

$$J_s = Z\beta^* N_0 \exp\left(\frac{-\Delta G^*}{kT}\right) \tag{B3}$$

In Eqs. (B2) and (B3), Z which stands for Zeldovich factor, β^* is the attachment rate of solute atoms to the precipitate (AL3X), N_0 denotes the number of nucleation sites available in the beginning, ΔG^* is the Gibbs energy of formation of a precipitate, k is Boltzmann's constant, and T is absolute temperature [12,13,32–38]. In Eq. (B2), θ can vary but in Thermo-Calc it is fixed at 2 [13].

The number density of precipitates, in the beginning, can be shown as in Eq. (B4), while the number density (N_t) at any instant of time (t) can be expressed as in Eq. (B5) [13]

$$N_0 \exp\left(\frac{-\Delta G^*}{kT}\right) \tag{B4}$$

$$N_t = \int J_t dt \tag{B5}$$

ΔG^* is the Gibbs energy (or activation energy) of formation of the precipitate can be expressed as in Eq. (B6). $\Delta G_m^{FCC-Al_3Sc}$ is the molar Gibbs energy of formation of Al_3Sc nanocrystals from the FCC matrix and $V_m^{Al_3Sc}$ is the molar volume of Al_3Sc nanocrystals [34], while σ is the interfacial energy between the FCC matrix phase and precipitate Al_3Sc phase

$$\Delta G^* = \frac{16\pi}{3} \frac{\sigma_{int}^3}{\left(\frac{\Delta G_m^{FCC-Al_3Sc}}{V_m^{Al_3Sc}}\right)^2} \tag{B6}$$

Zeldovich factor (Z) and β^* can be expressed as shown by Eqs. (B7) and (B8), respectively [13,39–41]

$$Z = \frac{V_m^{Al_3Sc}}{2\pi N_A R^{*2}} \sqrt{\frac{\sigma}{kT}} \tag{B7}$$

$$\beta^* = \frac{2\pi R^{*2}}{(l^{Al_3Sc})^4}\left[\sum \frac{(\overline{X_i^{Al_3Sc}} - \overline{X_i^{FCC}})^2}{\overline{X_i^{FCC}} D_i^{FCC}}\right]^{-1} \quad \text{(B8)}$$

In Eq. (B8), $\overline{X_i^{FCC}}$ and $\overline{X_i^{Al_3Sc}}$ are the equilibrium composition of element i in the FCC and in the Al_3Sc phase respectively, while D_i^{FCC} is the chemical diffusion coefficient of element i in the FCC phase [39–42].

For Al_3Sc crystals, critical radius (R^*) [30–33] and time-dependent radius ($R_t^{Al_3Sc}$) [41,42] can be expressed as in Eqs. (B9) and (B10), respectively.

$$R^* = -\frac{2\sigma V_m^{Al_3Sc}}{\Delta G_m^{FCC-Al_3Sc}} \quad \text{(B9)}$$

$$\frac{dR_t^{Al_3Sc}}{dt} = \frac{D_i^{FCC}}{\xi_{i,t} R_t^{Al_3Sc}} \frac{X_{i,t}^{FCC} - \overline{X_i^{FCC}}}{\overline{X_i^{Al_3Sc}} - \overline{X_i^{FCC}}} \quad \text{(B10)}$$

In Eq. (B10), $X_{i,t}^{FCC}$ is the composition of the supersaturated FCC matrix phase and $\overline{X_i^{Al_3Sc}}$ is the equilibrium composition of the Al_3Sc phase. The growth of Al_3Sc crystals is dependent $X_{i,t}^{FCC}$. Thus, the mass balance equation can be expressed as shown in Eq. (B11) [40]

$$X_{i,t}^{FCC} = (X_{i,0}^{FCC} - V_f^{Al_3Sc}\overline{X_i^{Al_3Sc}})/(1 - V_f^{Al_3Sc}) \quad \text{(B11)}$$

In Eq. (B10), parameter $\xi_{i,t}$ can be expressed as in Eq. (B12), while parameter $\lambda_{i,t}$ in Eq. (B12) can be calculated by solving Eq. (B13) [40–42]

$$\xi_{i,t} = 1 - \lambda_{i,t}\pi \exp(\lambda_{i,t}^2)\mathrm{erfc}(\lambda_{i,t}) = \frac{1}{2\lambda_{i,t}^2} \frac{X_{i,t}^{FCC} - \overline{X_i^{FCC}}}{\overline{X_i^{Al_3Sc}} - \overline{X_i^{FCC}}} \quad \text{(B12)}$$

$$2\lambda_{i,t}^2 - 2\lambda_{i,t}^3\sqrt{\pi}\exp(\lambda_{i,t}^2)erfc(\lambda_{i,t}) = \frac{X_{i,t}^{FCC} - \overline{X_i^{FCC}}}{\overline{X_i^{Al_3Sc}} - \overline{X_i^{FCC}}} \quad \text{(B13)}$$

Coarsening rate of the precipitate can be predicted from the growth equation shown in Eq. (B14) [42–44]

$$\frac{dR_t^{Al_3Sc}}{dt} = \frac{8}{27} \frac{\sigma V_{at}^{Al_3Sc}}{(R^{Al_3Sc})^2 kT} \frac{D_i^{FCC}\overline{X_i^{FCC}}}{\overline{X_i^{Al_3Sc}} - \overline{X_i^{FCC}}} \quad \text{(B14)}$$

In Eq. (B14), $V_{at}^{Al_3Sc}$ is the mean atomic volume of the Al_3Sc phase, while N_A is the Avogadro's number

$$V_{at}^{Al_3Sc} = \frac{V_m^{Al_3Sc}}{N_A} \quad \text{(B15)}$$

Time-dependent mean radius and volume fraction of Al_3Sc nanocrystals at any time step can be calculated through Eqs. (B16) and (B17), respectively [39–42]

$$\overline{R_t^{Al_3Sc}} = \frac{\sum N_t R_t^{Al_3Sc}}{\sum N_t} \quad \text{(B16)}$$

$$V_{f,t}^{Al_3Sc} = \sum N_t \frac{4\pi (R_t^{Al_3Sc})^3}{3} \quad \text{(B17)}$$

Appendix C

Johnson–Mehl–Avrami–Kolmogorov Analysis. During nucleation and growth, the volume fraction of a precipitate follows the JMAK equation shown in Eq. (C1) [45]

$$f_v(t) = f_{v0}\left(1 - \exp\left(-\frac{t}{t_r}\right)^n\right) \quad \text{(C1)}$$

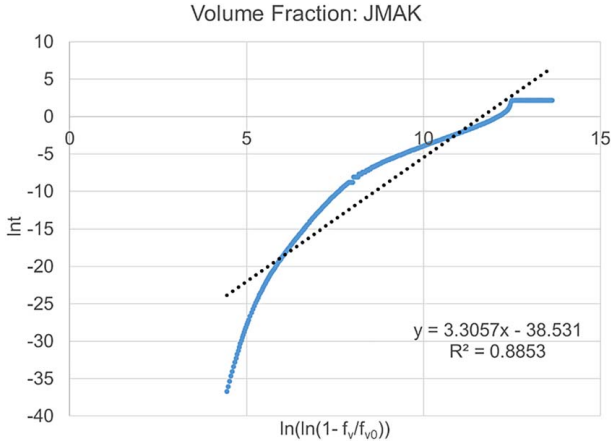

Fig. 8 JMAK analysis for volume fraction estimations

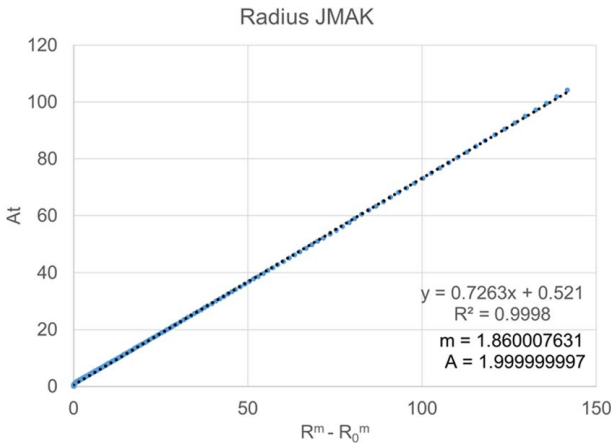

Fig. 9 JMAK analysis for estimation of the mean radius of the grain

JMAK analysis for estimating the evolution of the Al_3Sc phase has been analyzed for a better understanding of nucleation and growth phenomenon. Figure 8 shows the relevant plot for volume fraction, while Fig. 9 shows the relevant plot for the mean radius.

In Fig. 8, one can observe that a perfect straight line was not obtained as expected. In Fig. 9, a straight line can be observed.

As mentioned throughout this text, this is a completely new system. It was studied under the framework of the CALPHAD approach, where usually 3–6 elements are analyzed at a time. Thus, some discrepancies are unavoidable. Our group is working on improving model development within the framework of the CALPHAD approach and expects to improve the models to their maturity and use toward experiments.

References

[1] Røyset, J., and Ryum, N., 2005, "Scandium in Aluminium Alloys," Int. Mater. Rev., **50**(1), pp. 19–44.

[2] Dorin, T., Ramajayam, M., Babaniaris, S., Jiang, L., and Langan, T. J., 2019, "Precipitation Sequence in Al–Mg–Si–Sc–Zr Alloys During Isochronal Aging," Materialia, **8**, p. 100437.

[3] Thermo-Calc Software TCAL5: TCS Aluminium-based Alloys Database v.5, https://www.Thermo-Calc.com/media/56675/TCAL5-1_extended_info.pdf, Accessed August 30, 2019.

[4] De Luca, A., Dunand, D. C., and Seidman, D. N., 2018, "Scandium-Enriched Nanoprecipitates in Aluminum Providing Enhanced Coarsening and Creep Resistance," Light Metals 2018. Proceedings of the TMS 2018. International Symposium on Light Metals, Phoenix, AZ, Mar. 11–15, 2018, Springer International Publishing, pp. 1589–1594.
[5] Dorin, T., Ramajayam, M., Lamb, J., and Langan, T., 2017, "Effect of Sc and Zr Additions on the Microstructure/Strength of Al-Cu Binary Alloys," Mat. Sci. Eng. A-Struct., **707**, pp. 58–64.
[6] Mondol, S., Alam, T., Banerjee, R., Kumar, S., and Chattopadhyay, K., 2017, "Development of a High Temperature High Strength Al Alloy by Addition of Small Amounts of Sc and Mg to 2219 Alloy," Mat. Sci. Eng. A-Struct., **687**, pp. 221–231.
[7] Gao, Y. H., Cao, L. F., Kuang, J., Zhang, J. Y., Liu, G., and Sun, J., 2020, "Dual Effect of Cu on the Al3Sc Nanoprecipitate Coarsening," J. Mater. Sci. Technol., **37**, pp. 38–45.
[8] Zhang, C., Jiang, X., Zhang, R., Wang, X., Yin, H., Qu, X., and Liu, Z. K., 2019, "High-Throughput Thermodynamic Calculations of Phase Equilibria in Solidified 6016 Al-Alloys," Comput. Mater. Sci., **167**, pp. 19–24.
[9] Tang, K., Dua, Q., and Li, Y., 2018, "Modelling Microstructure Evolution During Casting, Homogenization and Ageing Heat Treatment of Al-Mg-Si-Cu-Fe-Mn Alloys," Calphad, **63**, pp. 164–184.
[10] Du, Q., Jia, L., Tang, K., and Holmedal, B., 2018, "Modelling and Experimental Validation of Microstructure Evolution During the Cooling Stage of Homogenization Heat Treatment of Al–Mg–Si Alloys," Materialia, **4**, pp. 70–80.
[11] Sarafoglou, P. I., Serafeim, A., Fanikos, I. A., Aristeidakis, J. S., and Haidemenopoulos, G. N., 2019, "Modeling of Microsegregation and Homogenization of 6xxx Al-Alloys Including Precipitation and Strengthening During Homogenization Cooling," Materials, **12**(9), p. 1421.
[12] Andersson, J. O., Helander, T., Höglund, L., Shi, P. F., and Sundman, B., 2002, "Thermo-calc and DICTRA, Computational Tools for Materials Science," Calphad, **26**(2), pp. 273–312.
[13] Thermo-Calc Software: The Precipitation Module (TC-PRISMA) User Guide 2018B, https://thermocalc.com/support/how-to-cite-thermo-calc-products/, Accessed August 30, 2019.
[14] Thermo-Calc Software MOBAL4: TCS Al-alloys Mobility Database, v4, https://thermocalc.com/support/how-to-cite-thermo-calc-products/, Accessed August 30, 2019.
[15] Jha, R., and Dulikravich, G. S., 2020, "Solidification and Heat Treatment Simulation for Aluminum Alloys With Scandium Addition," Comput. Mater. Sci., **182**, pp. 1–8.
[16] TensorFlow, https://www.tensorflow.org/, Accessed August 30, 2019.
[17] Keras: The Python Deep Learning library, https://keras.io/, Accessed August 30, 2019.
[18] Jha, R., and Dulikravich, G. S., 2019, "Design of High Temperature Ti-Al-Cr-V Alloys for Maximum Thermodynamic Stability," Metals, **9**(5), p. 537.
[19] Jha, R., and Dulikravich, G. S., 2021, "Discovery of New Ti-Based Alloys Aimed at Avoiding/Minimizing Formation of α" and ω-Phase Using CALPHAD and Artificial Intelligence," Metals, **11**(1), pp. 1–15.
[20] Jha, R., Dulikravich, G. S., Chakraborti, N., Fan, M., Schwartz, J., Koch, C., Colaco, M. J., Poloni, C., and Egorov, I. N., 2017, "Self-organizing Maps for Pattern Recognition in Design of Alloys," Mater. Manuf. Processes, **10**(10), pp. 1067–1074.
[21] Jha, R., Dulikravich, G. S., Colaco, M. J., Fan, M., Schwartz, J., and Koch, C. C., 2017, "Magnetic Alloys Design Using Multi-objective Optimization," *Properties and Characterization of Modern Materials*, 33, A. Oechsner, L. M. da Silva, and H. Altenbach, eds., Springer, Germany, pp. 261–284.
[22] Jha, R., Chakraborti, N., Diercks, D., Stebner, A., and Ciobanu, C. V., 2018, "Combined Machine Learning and CALPHAD Approach for Discovering Processing-Structure Relationships in Soft Magnetic Alloys," Comput. Mater. Sci., **150**, pp. 202–211.
[23] Jha, R., Diercks, D., Stebner, A., Ciobanu, C. V., and Chakraborti, N., 2019, "Interfacial Energy of Copper Clusters in Fe-Si-B-Nb-Cu Alloys," Scr. Mater., **162**, pp. 331–334.
[24] Jha, R., Pettersson, F., Dulikravich, G. S., Saxen, H., and Chakraborti, N., 2015, "Evolutionary Design of Nickel-Based Superalloys Using Data-Driven Genetic Algorithms and Related Strategies," Mater. Manuf. Process., **30**(4), pp. 488–510.
[25] Assadiki, A., Esin, V. A., Bruno, M., and Martinez, R., 2018, "Stabilizing Effect of Alloying Elements on Metastable Phases in Cast Aluminum Alloys by CALPHAD Calculations," Comput. Mater. Sci., **145**, pp. 1–7.
[26] Andersen, S. J., Marioara, C. D., Friis, J., Wenner, S., and Holmestad, R., 2018, "Precipitates in Aluminium Alloys," Adv. Phys.-X, **3**(1), p. 1479984.
[27] Kumar, S., and Padture, N. P., 2018, "Materials in the Aircraft Industry," *Metallurgical Design and Industry: Prehistory to the Space Age*, B Kaufman, and CL Briant, eds., Springer, Cham, Springer International Publishing AG, part of Springer Nature Switzerland AG, pp. 271–346.
[28] TensorBoard: TensorFlow's Visualization Toolkit, https://www.tensorflow.org/tensorboard, Accessed August 30, 2019.
[29] Haidemenopoulos, G. N., Katsamas, A. I., and Kamoutsi, H., 2010, "Thermodynamics-Based Computational Design of Al-Mg-Sc-Zr Alloys," Metall. Mater. Trans. A, **41**(4), pp. 888–899.
[30] Liu, J., Yao, P., Zhao, N., Shi, C., Li, H., Li, X., Xi, D., and Yang, S., 2016, "Effect of Minor Sc and Zr on Recrystallization Behavior and Mechanical Properties of Novel Al–Zn–Mg–Cu Alloys," J. Alloys Compd., **657**, pp. 717–725.
[31] Mochugovskiy, A. G., and Mikhaylovskaya, A. V., 2020, "Comparison of Precipitation Kinetics and Mechanical Properties in Zr and Sc-Bearing Aluminum-Based Alloys," Mater. Lett., **275**, p. 128096.
[32] Wagner, R., and Kampmann, R., 1991, "Homogeneous Second Phase Precipitation," *Materials Science and Technology, Vol. 5, Phase Transformations in Materials*, R. W. Cahn, P. Haasen, and E. J. Kramer, eds., VCH, Weinhein, Germany, p. 21.
[33] Kampmann, R., Eckerlebe, H., and Wagner, R., 2000, "Precipitation Kinetics in Metastable Solid Solutions-Theoretical Considerations and Application to Cu-Ti Alloys," Mater. Res. Soc. Symp. Proc. MRS, **57**, pp. 525–542.
[34] Cinkilic, E., Yan, X., and Luo, A. A., 2020, "Modeling Precipitation Hardening and Yield Strength in Cast Al-Si-Mg-Mn Alloys," Metals, **10**(10), p. 1356.
[35] Sarafoglou, P. I., Serafeim, A., Fanikos, I. A., Aristeidakis, J. S., and Haidemenopoulos, G. N., 2019, "Modeling of Microsegregation and Homogenization of 6xxx Al-Alloys Including Precipitation and Strengthening During Homogenization Cooling," Materials, **12**(9), p. 1421.
[36] Langer, J., and Schwartz, K., 1980, "Kinetics of Nucleation in Near-Critical Fluids," Phys. Rev. A, **21**(3), pp. 948–958.
[37] Russell, K. C., and Yamauchi, K., 1980, "Nucleation in Solids: the Induction and Steady State Effects," Adv. Colloid Interface Sci., **13**(3–4), pp. 205–318.
[38] Bardel, D., Perez, M., Nelias, D., Deschamps, A., Hutchinson, C. R., Maisonnette, D., Chaise, T., Garnier, J., and Bourlier, F., 2014, "Coupled Precipitation and Yield Strength Modelling for Non-Isothermal Treatments of a 6061 Aluminium Alloy," Acta Mater., **62**, pp. 129–140.
[39] Agren, J., 2015, "Nucleation—A Challenge in the Modelling of Phase Transformations," International Conference on Solid–Solid Phase Transformations in Inorganic Materials, Canada, June 28–July 3, pp. 9–14.
[40] Bonvalet, M., Philippe, T., Sauvage, X., and Blavette, D., 2015, "Modeling of Precipitation Kinetics in Multicomponent Systems: Application to Model Superalloys," Acta Mater., **100**, pp. 169–177.
[41] Chen, Q., Jeppsson, J., and Agren, J., 2008, "Analytical Treatment of Diffusion During Precipitate Growth in Multicomponent Systems," Acta Mater., **56**(8), pp. 1890–1896.
[42] Li, S., Kattner, U. R., and Campbell, C. E., 2017, "A Computational Framework for Material Design," Integr. Mater. Manuf. Innov., **6**(3), pp. 229–248.
[43] Rougier, L., Jacot, A., Gandin, C.-A., Di Napoli, P., Théry, P.-Y., Ponsen, D., and Jaquet, V., 2013, "Numerical Simulation of Precipitation in Multicomponent Ni-Base Alloys," Acta Mater., **61**(17), pp. 6396–6405.
[44] Perez, M., Dumont, M., and Acevedo-Reyes, D., 2008, "Implementation of Classical Nucleation and Growth Theories for Precipitation," Acta Mater., **56**(9), pp. 2119–2132.
[45] Avrami, M., 1941, "Kinetics of Phase Change. III. Granulation, Phase Change, and Microstructure," J. Chem. Phys., **9**(2), pp. 177–184.